Linking Electronic Transport through a Spin Crossover Thin Film to the Molecular Spin State Using X-ray Absorption Spectroscopy Operando Techniques

Filip Schleicher,[†,‡] Michał Studniarek,[†] Kuppusamy Senthil Kumar,[†] Etienne Urbain,[†] Kostantine Katcko,[†] Jinjie Chen,[§] Timo Frauhammer,[§] Marie Hervé,[§] Ufuk Halisdemir,[†] Lalit Mohan Kandpal,[†] Daniel Lacour,[‡] Alberto Riminucci,[∥] Loic Joly,[†] Fabrice Scheurer,[†] Benoit Gobaut,[⊥] Fadi Choueikani,[⊥] Edwige Otero,[⊥] Philippe Ohresser,[⊥] Jacek Arabski,[†] Guy Schmerber,[†] Wulf Wulfhekel,[§,#] Eric Beaurepaire,[†,∇] Wolfgang Weber,[†] Samy Boukari,[†] Mario Ruben,[†,#] and Martin Bowen*,[†]

[†]IPCMS, UMR 7504 CNRS, Université de Strasbourg, 23 Rue du Loess, BP 43, 67034 Strasbourg Cedex 2, France
[‡]Université de Lorraine, CNRS, IJL, F-54000 Nancy, France
[§]Physikalisches Institut, Karlsruhe Institute of Technology, Wolfgang-Gaede-Str. 1, 76131 Karlsruhe, Germany
[∥]ISMN-CNR, Via Gobetti 101, 40129 Bologna, Italy
[⊥]Synchrotron SOLEIL, L'Orme des Merisiers, Saint-Aubin, BP 48, 91192 Gif-sur-Yvette, France
[#]Institute of Nanotechnology, Karlsruhe Institute of Technology (KIT), Hermann-von-Helmholtz-Platz 1, 76344 Eggenstein-Leopoldshafen, Germany

S Supporting Information

ABSTRACT: One promising route toward encoding information is to utilize the two stable electronic states of a spin crossover molecule. Although this property is clearly manifested in transport across single molecule junctions, evidence linking charge transport across a solid-state device to the molecular film's spin state has thus far remained indirect. To establish this link, we deploy materials-centric and device-centric operando experiments involving X-ray absorption spectroscopy. We find a correlation between the temperature dependencies of the junction resistance and the Fe spin state within the device's $[Fe(H_2B(pz)_2)_2(NH_2\text{-phen})]$ molecular film. We also factually observe that the Fe molecular site mediates charge transport. Our dual operando studies reveal that transport involves a subset of molecules within an electronically heterogeneous spin crossover film. Our work confers an insight that substantially improves the state-of-the-art regarding spin crossover-based devices, thanks to a methodology that can benefit device studies of other next-generation molecular compounds.

KEYWORDS: spin crossover thin film, solid-state device, operando measurements, spintronics, X-ray absorption spectroscopy
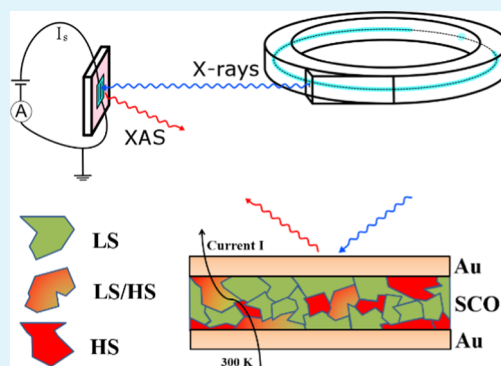
INTRODUCTION

A promising route to overcoming the miniaturization limits of traditional storage technologies involves the use of molecules whose conformation, and resulting electronic properties, can be switched between two stable states. One such family of molecular candidates is that of spin crossover (SCO) molecules,[1,2] in which the ligand field around a central metal ion may be reversibly altered so as to switch the atom's electronic configuration between low-spin (LS) and high-spin (HS) states. This conformational change occurs via external stimuli (e.g. temperature, light, electric field), which would confer multifunctionality to a SCO-based device.[3]

A substantial difficulty toward successfully assembling devices with a bistability inherited from a molecule's SCO property is that the electronically fragile SCO property can become frozen upon forming an interface with the device electrode. In particular, the large interfacial charge transfer that underscores this change can be mitigated by considering surfaces with a reduced density of states and/or reduced chemical activity.[4−6] The SCO transition temperature may also be manipulated through suitable surface engineering.[7−11]

Witnessing how the SCO property impacts a device's response has been explicitly achieved through experiments on model junctions assembled using the tip of a scanning

tunneling microscope.[2,3] However, transposing this level of knowledge to solid-state device research, i.e., with industrial prospects, has remained challenging.[1,3] A few reports of device research involving SCO molecules have provided phenomenological modeling of experimental transport data to support a picture of thermal,[12−15] electrical field,[16] or optical[17] SCO-induced changes to device operation. However, an explicit link between electronic transport and the actual fraction ρ_{HS} of molecules in the HS state within the device, let alone within the actual charge transport path across the SCO film, has, to the best of our knowledge, not yet been demonstrated.

Establishing this link is best achieved through an in operando technique. Two approaches are possible. In a so-called "materials-centric" operando approach, the device is placed in a given state and the materials property is read out through the standard materials science method. However, the atoms probed by this materials science technique do not necessarily contribute equally to a device's operation. To improve causality between materials science and device research, a "device-centric" operando approach can focus this materials characterization onto those atoms that drive the device's operation by examining the materials property within device operation (e.g., current flow).[18]

In this article, we use synchrotron-grade materials-centric and device-centric operando measurements[18] combining the element specificity of X-ray absorption spectroscopy (XAS) and electrical transport to examine how the thermally activated spin transition impacts transport across a vertical crossbar device based on the generic $[Fe(H_2B(pz)_2)_2(phen)]$ (bpz = dihydrobis(pyrazolyl)borate, phen = 1,10-phenanthroline) family of molecules. Using the materials-centric technique, we find that the temperature dependence of the fraction ρ_{HS} of molecules in the HS state within a $Au/[Fe(H_2B(pz)_2)_2(NH_2-phen)]/Au$ trilayer, extracted from XAS measurements, tracks the temperature dependence of junction resistance. Device-centric operando measurements confirm that the Fe central site is involved in transport, and shed light on the subset of SCO molecules that are actually involved in SCO-driven transport across the electronically heterogeneous SCO film.

■ EXPERIMENTAL SECTION

We chose the $[Fe(H_2B(pz)_2)_2(phen)]$ family of molecules because not only can they be sublimed,[19] but it also shows a high degree of functionalization potential, and its members can be synthesized using easily accessible and inexpensive precursors. The molecule studied in this work is $[Fe(H_2B(pz)_2)_2(NH_2-phen)]$, with NH$_2$-phen = 5-amino1,10-phenanthroline (see inset to Figure 1a). Thanks to the addition of the NH$_2$ functional group, the studied compound may easily act as a frame for the realization of functional SCO molecules. Details of the molecular synthesis are described in Supporting Information Note 1. We show in Figure 1a the temperature dependence of the magnetization ($\chi_m T$) of a powder reference acquired using superconducting quantum interference device magnetometry (SQUID) upon cooldown and warm-up. SQUID magnetometry shows a nearly vanishing $\chi_m T$ at low temperatures that reflects the nonmagnetic ($S = 0$) LS state and a thermal SCO to the HS state at a critical transition temperature of 154 K for the bulk powder without any apparent thermal hysteresis (ΔT).

Trilayer device stacks incorporating $[Fe(H_2B(pz)_2)_2(NH_2-phen)]$ molecules were fabricated on thermally oxidized Si/SiO$_x$ substrates. Before the deposition, the substrates were cleaned in an oxygen plasma. The entire structure consisted of Au(20 nm)/[Fe(H$_2$B-(pz)$_2$)$_2$(NH$_2$-phen)](42 nm)/Au(20 nm) in which the Au electrodes were evaporated in UHV through a shadow mask, with ex situ transfer to a current-heated crucible molecular evaporator. Molecules were
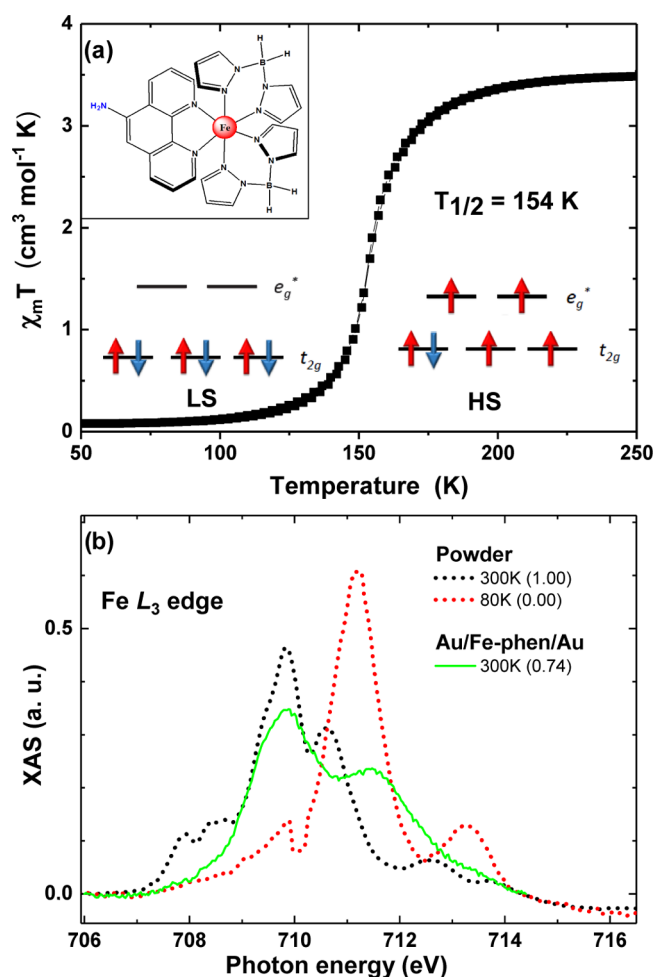
Figure 1. (a) $\chi_m T$ vs T plot of the $[Fe(H_2B(pz)_2)_2(NH_2-phen)]$ powder reference and corresponding electronic configuration for the HS and LS state. (b) X-ray absorption spectra at the Fe L$_3$ edge of the powder reference in the HS state (at 300 K, black; $\rho_{HS} \equiv 1$) and LS state (at 70 K, red; $\rho_{HS} \equiv 0$) and of the Au/[Fe(H$_2$B(pz)$_2$)$_2$(NH$_2$-phen)]/Au trilayer at 300 K (green line) for which a value of the trilayer ρ_{HS} = 0.74 is extracted by using the peak intensity ratio method (see Supporting Information Note 2).

sublimed at a pressure $P = 4.3 \times 10^{-8}$ mbar without the mask and covered the entire sample. The intersection between the bottom and top Au electrodes with a respective width of 300 and 50 μm thus defined the junctions. This junction size represents a compromise between a reasonably high device resistance (typically ~6 MΩ at low bias) and continuity of electrodes evaporated through the mask atop the SCO film.

The device was measured on the DEIMOS beamline[20] of Synchrotron SOLEIL using the V2TI electrical insert.[21] Junctions were bonded in a 2-point mode and measured using a Keithley 2636 sourcemeter in voltage source mode. The X-ray beam impinged normal to the sample surface. The data of Figure 2 were acquired in a materials-centric[18] operando mode: we witnessed the impact of varying the sample temperature on the SCO property by monitoring the XAS through total fluorescence yield (TFY) at the Fe L$_3$ edge and by measuring the junction resistance independently. Because molecules cover the entire sample surface, and because the 600 × 800 μm^2 X-ray beam cannot fit within the 300 × 50 μm^2 junction size, to probe only molecules that are sandwiched between Au electrodes, the materials-centric XAS data were acquired atop a mm-sized trilayer stack next to the junction. Thus, in this case, X-rays are not impinging upon the junction during transport measurements.
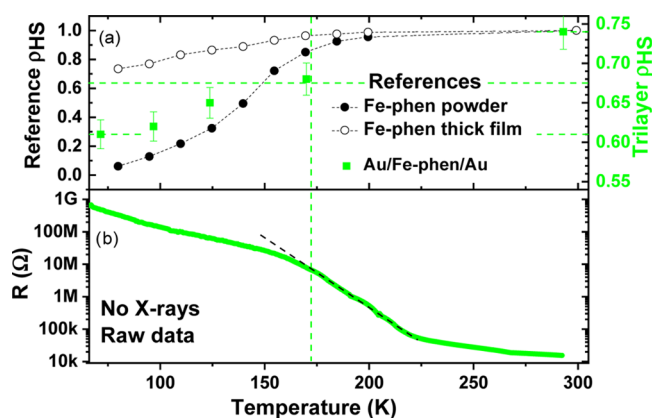
Figure 2. Temperature dependencies of (a) the HS proportion ρ_{HS} in a Au/[Fe(H$_2$B(pz)$_2$)$_2$(NH$_2$-phen)]/Au trilayer(green), a [Fe(H$_2$B-(pz)$_2$)$_2$(NH$_2$-phen)] reference powder (filled black), and a 230 nm thick [Fe(H$_2$B(pz)$_2$)$_2$(NH$_2$-phen)] film deposited onto Au (open black), and (b) of the Au/[Fe(H$_2$B(pz)$_2$)$_2$(NH$_2$-phen)]/Au device resistance R. The error bars of the reference ρ_{HS} data sets are masked by the symbol. To ensure a measurable current at all temperatures, a voltage of 800 mV was applied. The green dashed lines peg the ~170 K temperature at which the trilayer ρ_{HS} has decreased by half of its total amplitude due to the thermally activated SCO. This coincides with a deviation in $R(T)$ from the exponential dependence of $R(T > 170$ K) (intersection of vertical dashed green line with black dashed line).

We present in Figure 1b Fe L$_3$ edge XAS reference powder spectra in the HS (300 K, black dots; $\rho_{HS} \equiv 1$) and LS (80 K, red dots; $\rho_{HS} \equiv 0$) states. These spectra exhibit peaks at 709.8 and 711.3 eV corresponding to Fe t$_{2g}$4e$_g$2 ($S = 2$) and t$_{2g}$6e$_g$0 ($S = 0$) configurations for HS and LS molecules, respectively.[22] We also show a XAS spectrum acquired at 300 K on the Au/[Fe(H$_2$B(pz)$_2$)$_2$(NH$_2$-phen)]/Au trilayer (green line) after subtracting a baseline. By fitting this spectrum using a peak intensity ratio method based on the HS and LS reference spectra of the powder sample, we extracted a proportion ρ_{HS} of molecules in the HS state of 0.74 at 300 K for molecules sandwiched between Au electrodes in our devices[11] (see Supporting Information Note 2). By repeating this fitting procedure on the XAS spectra acquired on the reference SCO junction upon varying the sample temperature, we can then extract the temperature dependence of the trilayer ρ_{HS} for molecules sandwiched between Au electrodes. We plot it in Figure 2a (green squares), alongside the temperature dependence of the reference ρ_{HS} for both the powder sample (filled dots) and a 230 nm thick film deposited on gold (open black dots).

We find that, at room temperature, $\rho_{HS} = 0.74$, i.e., only 74% of the molecules sandwiched between gold electrodes are in the HS state, whereas at 70 K ρ_{HS} drops to 0.61. This suggests that only 13% of the molecules actually switch, implying that the remaining molecules are blocked in the HS and LS states (61 and 26%, respectively). Also, ρ_{HS} only reaches 0.75 at 80 K in the thick reference film deposited on gold, whereas it is ~0 at 80 K for the powder. This can arise from the aforementioned electronic coupling to the gold electrodes,[23−26] or from modified intermolecular interactions in the molecular film,[27] or from potential structural degradation issues. These aspects can also account for the different transition temperatures observed in the powder, the thick film deposited on gold, and the thin film sandwiched between Au electrodes.[11,28] Finally, the gradual character of the transition suggests reduced cooperativity of the molecules with respect to the powder sample.[8,27,29,30]

Turning now to Figure 2b, the SCO device resistance R generally increases as temperature decreases (note the resistance log scale used). Starting from 300 K, this increase is nearly exponential, which is typical of thermally assisted hopping transport across a SCO organic layer.[13] Starting at roughly 220 K, this exponential increase

becomes steeper but is arrested around 175 K. It is also at this temperature that the trilayer ρ_{HS} decreased by half its total amplitude (see dashed lines in panels (a) and (b) of Figure 2). For temperatures lower than around 175 K, another exponential dependence appears to drive the temperature dependence of R. The data also suggest that, setting aside thermally assisted hopping, the LS state R is lower than the HS state R, in line with other studies.[13,17,31] Bear in mind, however, that the relative resistances of the LS and HS states may depend on the applied bias amplitude and the selected molecule.[32] These considerations apply to thermally switchable molecules, not those that are frozen in a HS or LS state (see hereafter).

This comparison between the temperature dependencies of ρ_{HS} and of device resistance in terms of two HS- and LS-dominated transport regimes thus suggests that transport across the junction indeed involves the SCO property. However, because the XAS-based determination of ρ_{HS} remains materials-centric, it does not explicitly probe the spin state of the molecules that form the actual charge transport path across the SCO film. To further support this claim of SCO-driven operation, we examine in a device-centric operando approach[18] if the Fe site of the [Fe(H$_2$B(pz)$_2$)$_2$(NH$_2$-phen)] SCO molecule is involved in transport. To do so, we positioned the X-ray beam on the junction and swept the photon energy across the Fe L edge while simultaneously measuring TFY (see Figure 3a) and the raw current I flow across the junction for ±10 mV (see Figure 3b) at $T = 300$ K.
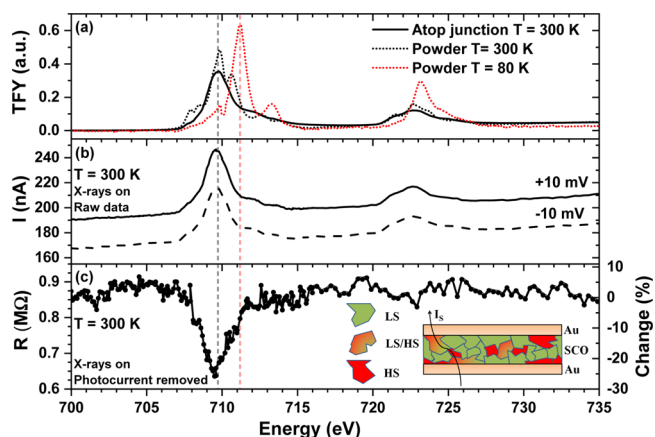
Figure 3. Impact at $T = 300$ K of sweeping photon energy across the Fe L$_3$ edge on (a) X-ray absorption spectra (black line) measured on the $300 \times 50\ \mu m^2$ Au/[Fe(H$_2$B(pz)$_2$)$_2$(NH$_2$-phen)]/Au junction in TFY mode with a $800 \times 600\ \mu m^2$ X-ray beam, and on (b) the current I flowing across the device for both signs of 10 mV applied bias, i.e., in a device-centric operando approach.[18] The HS state witnessed in the TFY spectrum of panel (a) corroborates data for the thick SCO reference film of Figure 2a. Panel (a) also shows the reference powder spectra in the HS (black dots) and LS (red dots) states. The same sign of effective current for $V = \pm10$ mV reflects the sizeable photocurrent here. (c) Impact of Fe L$_3$ edge absorption on the device resistance after removing the photocurrent. The resistance R at 300 K changes by 25% upon reaching the Fe L$_3$ edge. This 0.25 MΩ change exceeds the 0.025 MΩ noise level observed in the pre-edge region by a factor of 10. We observe a maximum at 709.8 eV corresponding to the HS state, but no LS state-induced spectral weight at 711.2 eV. This spectrum cannot be explained in terms of either a trivial photocarrier contribution from the entire illuminated region (see Supporting Information Note 3) or from within the junction (compare with Figure 1b). Transport is therefore sensitive only to HS state molecules at 300 K. The inset to panel (c) schematizes how the current (black arrow) flows across HS sites that are either frozen (red zones) or switchable (red/green zones) at 300 K and not across frozen LS sites (green zones).

Both the TFY and raw junction current spectra clearly reveal the impact of X-ray absorption by Fe sites. Given the respective 800×600 and 300×50 μm^2 sizes of the X-ray beam and the junction, molecules outside the junction contribute 98% weight to the TFY spectrum of Figure 3a. This is why the TFY spectrum corroborates the data for the thick reference SCO film of Figure 2a. Because the sample is grounded through our IV measurement unit, this also means that the raw current spectra of panel (b) naturally include a photocurrent resulting from the absorption of X-rays by Fe sites belonging to molecules that are almost entirely outside the junction. This photocurrent is large enough to promote the same sign of junction current for $V = \pm 10$ mV. To remove this photocurrent, originating both around and within the junction, so as to concentrate on device transport, we apply a previously tested methodology:[18] we assume a bias-symmetric operation at low bias and subtract the two ± 10 mV raw current spectra of panel (b) using the formula $R = 2V/[(I_{+10mV}) - (I_{-10mV})]$. The resulting photon energy dependence of device resistance, with sample/device photocurrent removed, is plotted in Figure 3c. We find a 25% drop in device resistance $R(E)$ upon sweeping across the Fe L edge.

We deduce from three observations that this is not a trivial photocarrier effect. (1) Any subtle difference in the background and/or efficiency of photocurrent generation between our raw +10 and −10 mV measurements (Figure 3b) would generate a slope on the background of our corrected resistance data (Figure 3c), which we do not observe (witness how $R(700 \text{ eV}) \approx R(735 \text{ eV})$). (2) As shown in Supporting Information Note 3, $R(E)$ (Figure 3c) does not track the energy dependence of the photocurrent and also cannot be fitted using the TFY data of Figure 3a that was acquired simultaneously with the raw device current (Figure 3b). (3) In the first demonstration[18] of device operation in an X-ray excited state, we found that the resistance of MgO-based magnetic tunnel junctions may increase or decrease depending on its magnetic state. To explain the resistance increase, we extended an already mature understanding of conventional solid-state tunneling transport. Because an understanding of conventional transport across SCO thin films is comparatively much less mature, we refrain from speculating on how the SCO device operates in the X-ray excited state at this stage. This nevertheless indicates that illuminating a device with soft X-rays shall not necessarily promote a resistance decrease.

(4) Because the electric field generated from the 10 mV applied across our 42 nm thick film is nearly 4 orders of magnitude lower than that required to electrically switch the spin state,[5] we expect no change in the spin state induced by operating the device. We may thus compare these device-centric (Figure 3c) and materials-centric (Figure 1b) operando results. We see that, although the trilayer ρ_{HS} = 0.74 at $T = 300$ K due to spectral weight at 711.2 eV (see Figure 1b), i.e., that the film contains 26% of molecules in the LS state, we do not observe any spectral weight at 711.2 eV in the $R(E)$ spectrum at $T = 300$ K of Figure 3c associated with the LS state, but only a peak at 709.8 eV that corresponds to the HS state.[33] This is incompatible with an interpretation in terms of photocarriers solely within the device, for which the LS/HS spectral weight of both the XAS (Figure 1b) and $R(E)$ (Figure 3c) data would have been similar.

Because the device resistance changes upon sweeping across the Fe L edge and is not a photocarrier effect, this indicates that the Fe site is involved in transport across the SCO thin film. Because the Fe site carries the SCO property, this factually links transport with the SCO property. Furthermore, if we make the reasonable assumption that transport across a Fe site will be modified upon X-ray excitation regardless of its spin state, we find that the transport path at $T = 300$ K involves only molecules in the HS state. At low temperature, the raw device resistance was unmeasurable at the low 10 mV bias required[18] by the device-centric operando technique. We were thus unable to characterize the transport path at low temperature. Nevertheless, as mentioned before regarding thermally switchable molecules, the LS R is reported[2] to be lower than the HS R, and ρ_{HS} = 0.74 at $T = 300$ K within the trilayer according to the materials-centric operando data (see Figure 1b). Combining information accrued from our materials-centric and device-centric operando experiments, we

draw the following picture of the heterogeneous electronic and transport properties across the Au/[Fe(H$_2$B(pz)$_2$)$_2$(NH$_2$-phen)]/Au junction. (1) A 0.26 proportion of molecules is frozen in the LS state at $T = 300$ K and does not contribute to device operation. (2) Of the 0.74 proportion of Fe sites in the HS state at $T = 300$ K, only a 0.13 proportion manifests the SCO property (i.e., is thermally switchable), whereas a 0.61 proportion of molecules remains frozen in the HS state. As mentioned before, this freezing of the spin state into LS and HS configurations can arise from electronic coupling to the gold electrodes, from modified intermolecular interactions, and also potentially from structural degradation. (3) Transport at 300 K proceeds across molecules in the HS state (see inset in Figure 3c). (4) Although molecules that are in the frozen HS state could be contributing here, we witness how only a 0.13 thermally driven reduction to ρ_{HS}, which probes all Fe sites, can nevertheless heavily impact the temperature dependence of the junction resistance. The transport path therefore contains molecules with an active SCO property (see red/green zones within nanoscale transport path schematized in Figure 3c).

■ CONCLUSIONS

In conclusion, using X-ray absorption spectroscopy (XAS), we performed a material-centric and device-centric operando study on junctions integrating a [Fe(H$_2$B(pz)$_2$)$_2$(NH$_2$-phen)] spin crossover thin film. Using materials-centric XAS scans, we extracted the temperature dependence $\rho_{HS}(T)$ of the high-to-low spin ratio for a [Fe(H$_2$B(pz)$_2$)$_2$(NH$_2$-phen)] film sandwiched between Au electrodes. We find that $\rho_{HS}(T)$ can explain features of the junction resistance's temperature dependence directly in terms of the high-to-low spin ratio of molecules between the Au electrodes. Using the device-centric XAS operando technique, we confirmed the involvement of Fe sites within the charge transport path across the vertical device's SCO layer. By comparing the materials-centric and device-centric data, we qualitatively establish a picture of SCO-driven transport across a subset of molecules forming the electronically heterogeneous SCO film within the device's trilayer structure, with an insight that substantially improves the state-of-the-art regarding SCO-based solid-state device knowledge. Our work should stimulate further studies, within a challenging context, to enhance the impact of the SCO property on the operation/performance of solid-state devices. A particularly promising prospect remains to successfully combine the SCO property with the high spin polarization at the ferromagnet/molecule interface,[34] e.g., by tailoring the charge transfer thanks to a suitable noble metal spacer.[35] Finally, our work outlines a powerful methodology to examine how the operation of solid-state devices is impacted by the properties of next-generation molecular compounds incorporated therein.

■ ASSOCIATED CONTENT

⑤ Supporting Information
The Supporting Information is available free of charge on the ACS Publications website at DOI: 10.1021/acsami.8b11495.

Synthesis of [Fe(H$_2$B(pz)$_2$)$_2$(NH$_2$-phen)], HS/LS ratio determination, photocarrier hypothesis (PDF)

■ AUTHOR INFORMATION

Corresponding Author
*E-mail: bowen@unistra.fr.

ORCID ⓞ
Filip Schleicher: 0000-0003-3630-7285

Jinjie Chen: 0000-0003-4632-1988
Benoit Gobaut: 0000-0002-4086-8774
Wolfgang Weber: 0000-0002-9264-4537

Notes

■ ACKNOWLEDGMENTS

■ REFERENCES

(1) Molnár, G.; Rat, S.; Salmon, L.; Nicolazzi, W.; Bousseksou, A. Spin Crossover Nanomaterials: From Fundamental Concepts to Devices. *Adv. Mater.* **2017**, No. 17003862.

(2) Kumar, K. S.; Ruben, M. Emerging Trends in Spin Crossover (SCO) Based Functional Materials and Devices. *Coord. Chem. Rev.* **2017**, 346, 176−205.

(3) Lefter, C.; Davesne, V.; Salmon, L.; Molnár, G.; Demont, P.; Rotaru, A.; Bousseksou, A. Charge Transport and Electrical Properties of Spin Crossover Materials: Towards Nanoelectronic and Spintronic Devices. *Magnetochemistry* **2016**, 2, No. 18.

(4) Bernien, M.; Wiedemann, D.; Hermanns, C. F.; Krüger, A.; Rolf, D.; Kroener, W.; Müller, P.; Grohmann, A.; Kuch, W. Spin Crossover in a Vacuum-Deposited Submonolayer of a Molecular Iron(II) Complex. *J. Phys. Chem. Lett.* **2012**, 3, 3431−3434.

(5) Miyamachi, T.; Gruber, M.; Davesne, V.; Bowen, M.; Boukari, S.; Joly, L.; Scheurer, F.; Rogez, G.; Yamada, T. K.; Ohresser, P.; et al. Robust Spin Crossover and Memristance across a Single Molecule. *Nat. Commun.* **2012**, 3, No. 938.

(6) Bairagi, K.; Iasco, O.; Bellec, A.; Kartsev, A.; Li, D.; Lagoute, J.; Chacon, C.; Girard, Y.; Rousset, S.; Miserque, F.; et al. Molecular-Scale Dynamics of Light-Induced Spin Cross-over in a Two-Dimensional Layer. *Nat. Commun.* **2016**, 7, No. 12212.

(7) Zhang, X.; Costa, P. S.; Hooper, J.; Miller, D. P.; N'Diaye, A. T.; Beniwal, S.; Jiang, X.; Yin, Y.; Rosa, P.; Routaboul, L.; et al. Locking and Unlocking the Molecular Spin Crossover Transition. *Adv. Mater.* **2017**, 29, No. 1702257.

(8) Davesne, V.; Gruber, M.; Studniarek, M.; Doh, W. H.; Zafeiratos, S.; Joly, L.; Sirotti, F.; Silly, M. G.; Gaspar, A. B.; Real, J. A.; et al. Hysteresis and Change of Transition Temperature in Thin Films of Fe{[Me$_2$ Pyrz]$_3$ BH}$_2$, a New Sublimable Spin-Crossover Molecule. *J. Chem. Phys.* **2015**, 142, No. 194702.

(9) Mikolasek, M.; Félix, G.; Nicolazzi, W.; Molnár, G.; Salmon, L.; Bousseksou, A. Finite Size Effects in Molecular Spin Crossover Materials. *New J. Chem.* **2014**, 38, 1834−1839.

(10) Félix, G.; Nicolazzi, W.; Salmon, L.; Molnár, G.; Perrier, M.; Maurin, G.; Larionova, J.; Long, J.; Guari, Y.; Bousseksou, A. Enhanced Cooperative Interactions at the Nanoscale in Spin-Crossover Materials with a First-Order Phase Transition. *Phys. Rev. Lett.* **2013**, 110, No. 235701.

(11) Kumar, K. S.; Studniarek, M.; Heinrich, B.; Arabski, J.; Schmerber, G.; Bowen, M.; Boukari, S.; Beaurepaire, E.; Dreiser, J.; Ruben, M. Engineering On-Surface Spin Crossover: Spin-State Switching in a Self-Assembled Film of Vacuum-Sublimable Functional Molecule. *Adv. Mater.* **2018**, 30, No. 1705416.

(12) Shi, S.; Schmerber, G.; Arabski, J.; Beaufrand, J.-B.; Kim, D. J.; Boukari, S.; Bowen, M.; Kemp, N. T.; Viart, N.; Rogez, G.; et al. Study of Molecular Spin-Crossover Complex Fe(Phen)2(NCS)2 Thin Films. *Appl. Phys. Lett.* **2009**, 95, No. 043303.

(13) Devid, E. J.; Martinho, P. N.; Kamalakar, M. V.; Šalitroš, I.; Prendergast, Ú.; Dayen, J.-F.; Meded, V.; Lemma, T.; González-Prieto, R.; Evers, F.; et al. Spin Transition in Arrays of Gold Nanoparticles and Spin Crossover Molecules. *ACS Nano* **2015**, 9, 4496−4507.

(14) Takahashi, K.; Cui, H.-B.; Okano, Y.; Kobayashi, H.; Einaga, Y.; Sato, O. Electrical Conductivity Modulation Coupled to a High-Spin−Low-Spin Conversion in the Molecular System [Fe^{III} (Qsal)$_2$][Ni(Dmit)$_2$]$_3$·CH$_3$CN·H$_2$O. *Inorg. Chem.* **2006**, 45, 5739−5741.

(15) Prins, F.; Monrabal-Capilla, M.; Osorio, E. A.; Coronado, E.; van der Zant, H. S. J. Room-Temperature Electrical Addressing of a Bistable Spin-Crossover Molecular System. *Adv. Mater.* **2011**, 23, 1545−1549.

(16) Meded, V.; Bagrets, A.; Fink, K.; Chandrasekar, R.; Ruben, M.; Evers, F.; Bernand-Mantel, A.; Seldenthuis, J. S.; Beukman, A.; van der Zant, H. S. J. Electrical Control over the Fe(II) Spin Crossover in a Single Molecule: Theory and Experiment. *Phys. Rev. B* **2011**, 83, No. 245415.

(17) Lefter, C.; Rat, S.; Costa, J. S.; Manrique-Juárez, M. D.; Quintero, C. M.; Salmon, L.; Séguy, I.; Leichle, T.; Nicu, L.; Demont, P.; et al. Current Switching Coupled to Molecular Spin-States in Large-Area Junctions. *Adv. Mater.* **2016**, 28, 7508−7514.

(18) Studniarek, M.; Halisdemir, U.; Schleicher, F.; Taudul, B.; Urbain, E.; Boukari, S.; Hervé, M.; Lambert, C.-H.; Hamadeh, A.; Petit-Watelot, S.; et al. Probing a Device's Active Atoms. *Adv. Mater.* **2017**, 29, No. 1606578.

(19) Naggert, H.; Bannwarth, A.; Chemnitz, S.; von Hofe, T.; Quandt, E.; Tuczek, F. First Observation of Light-Induced Spin Change in Vacuum Deposited Thin Films of Iron Spin Crossover Complexes. *Dalton Trans.* **2011**, 40, 6364−6366.

(20) Ohresser, P.; Otero, E.; Choueikani, F.; Chen, K.; Stanescu, S.; Deschamps, F.; Moreno, T.; Polack, F.; Lagarde, B.; Daguerre, J.-P.; et al. DEIMOS: A Beamline Dedicated to Dichroism Measurements in the 350−2500 EV Energy Range. *Rev. Sci. Instrum.* **2014**, 85, No. 013106.

(21) Joly, L.; Muller, B.; Sternitzky, E.; Faullumel, J.-G.; Boulard, A.; Otero, E.; Choueikani, F.; Kappler, J.-P.; Studniarek, M.; Bowen, M.; et al. Versatile Variable Temperature Insert at the DEIMOS Beamline for in Situ Electrical Transport Measurements. *J. Synchrotron Radiat.* **2016**, 23, 652−657.

(22) Bernien, M.; Naggert, H.; Arruda, L. M.; Kipgen, L.; Nickel, F.; Miguel, J.; Hermanns, C. F.; Krüger, A.; Krüger, D.; Schierle, E.; et al. Highly Efficient Thermal and Light-Induced Spin-State Switching of an Fe(II) Complex in Direct Contact with a Solid Surface. *ACS Nano* **2015**, 9, 8960−8966.

(23) Gruber, M.; Miyamachi, T.; Davesne, V.; Bowen, M.; Boukari, S.; Wulfhekel, W.; Alouani, M.; Beaurepaire, E. Spin Crossover in Fe(Phen)$_2$ (NCS)$_2$ Complexes on Metallic Surfaces. *J. Chem. Phys.* **2017**, 146, No. 092312.

(24) Gopakumar, T. G.; Bernien, M.; Naggert, H.; Matino, F.; Hermanns, C. F.; Bannwarth, A.; Mühlenberend, S.; Krüger, A.; Krüger, D.; Nickel, F.; et al. Spin-Crossover Complex on Au(111): Structural and Electronic Differences Between Mono- and Multilayers. *Chem. - Eur. J.* **2013**, 19, 15702−15709.

(25) Shepherd, H. J.; Molnár, G.; Nicolazzi, W.; Salmon, L.; Bousseksou, A. Spin Crossover at the Nanometre Scale. *Eur. J. Inorg. Chem.* **2013**, 2013, 653−661.

(26) Beniwal, S.; Zhang, X.; Mu, S.; Naim, A.; Rosa, P.; Chastanet, G.; Létard, J.-F.; Liu, J.; Sterbinsky, G. E.; Arena, D. A.; et al. Surface-

Induced Spin State Locking of the [Fe(H$_2$B(Pz)$_2$)$_2$ (Bipy)] Spin Crossover Complex. *J. Phys.: Condens. Matter* **2016**, *28*, No. 206002.

(27) Naggert, H.; Rudnik, J.; Kipgen, L.; Bernien, M.; Nickel, F.; Arruda, L. M.; Kuch, W.; Näther, C.; Tuczek, F. Vacuum-Evaporable Spin-Crossover Complexes: Physicochemical Properties in the Crystalline Bulk and in Thin Films Deposited from the Gas Phase. *J. Mater. Chem. C* **2015**, *3*, 7870−7877.

(28) Shalabaeva, V.; Ridier, K.; Rat, S.; Manrique-Juarez, M. D.; Salmon, L.; Séguy, I.; Rotaru, A.; Molnár, G.; Bousseksou, A. Room Temperature Current Modulation in Large Area Electronic Junctions of Spin Crossover Thin Films. *Appl. Phys. Lett.* **2018**, *112*, No. 013301.

(29) Gütlich, P.; Hauser, A.; Spiering, H. Thermal and Optical Switching of Iron(II) Complexes. *Angew. Chem., Int. Ed. Engl.* **1994**, *33*, 2024−2054.

(30) Kipgen, L.; Bernien, M.; Ossinger, S.; Nickel, F.; Britton, A. J.; Arruda, L. M.; Naggert, H.; Luo, C.; Lotze, C.; Ryll, H.; et al. Evolution of Cooperativity in the Spin Transition of an Iron(II) Complex on a Graphite Surface. *Nat. Commun.* **2018**, *9*, No. 2984.

(31) Studniarek, M. Interface and Multifunctional Device Spintronics: Studies with Synchrotron Radiation. Ph.D. Thesis, Université de Strasbourg: Strasbourg, 2016.

(32) Jasper-Toennies, T.; Gruber, M.; Karan, S.; Jacob, H.; Tuczek, F.; Berndt, R. Robust and Selective Switching of an Fe^{III} Spin-Crossover Compound on Cu$_2$N/Cu(100) with Memristance Behavior. *Nano Lett.* **2017**, *17*, 6613−6619.

(33) The absence of a visible resistance drop at the Fe L$_2$ edge in Figure 3c likely reflects the lower L$_2$ amplitude and the signal-to-noise ratio of our resistance data.

(34) Djeghloul, F.; Gruber, M.; Urbain, E.; Xenioti, D.; Joly, L.; Boukari, S.; Arabski, J.; Bulou, H.; Scheurer, F.; Bertran, F.; et al. High Spin Polarization at Ferromagnetic Metal−Organic Interfaces: A Generic Property. *J. Phys. Chem. Lett.* **2016**, *7*, 2310−2315.

(35) Gruber, M.; Ibrahim, F.; Boukari, S.; Joly, L.; Da Costa, V.; Studniarek, M.; Peter, M.; Isshiki, H.; Jabbar, H.; Davesne, V.; et al. Spin-Dependent Hybridization between Molecule and Metal at Room Temperature through Interlayer Exchange Coupling. *Nano Lett.* **2015**, *15*, 7921−7926.